

Simple models for 2D tunable colloidal crystals in rotating AC Electric fields

Nils Elsner, C. Patrick Royall,* and Brian Vincent

School of Chemistry, University of Bristol, Bristol BS8 1TS, UK[†]

David R.E. Snoswell

Department of Physics, Cavendish Laboratory, University of Cambridge,

J.J. Thomson Avenue, Cambridge CB3 0HE, UK

(Dated: September 7, 2018)

Abstract

We compare the behaviour of a new 2D aqueous colloidal model system with a simple numerical treatment. To first order the attractive interaction between the colloids induced by an in-plane rotating AC electric field is dipolar, while the charge stabilisation leads to a shorter ranged, Yukawa-like repulsion. In the crystal-like ‘rafts’ formed at sufficient field strengths, we find quantitative agreement between experiment and Monte Carlo simulation, except in the case of strongly interacting systems, where the well depth of the effective potential exceeds 250 times the thermal energy. The ‘lattice constant’ of the crystal-like raft is located approximately at the minimum of the effective potential, resulting from the sum of the Yukawa and dipolar interactions. The experimental system has display applications, owing to the possibility of tuning the lattice spacing with the external electric field. Limitations in the applied field strength and relative range of the electrostatic interactions of the particles results in a reduction of tunable lattice spacing for small and large particles respectively. The optimal particle size for maximising the lattice spacing tunability was found to be around 1000 nm.

PACS numbers: 82.70.Dd

I. INTRODUCTION

Colloidal suspensions present the possibility to develop novel materials via self-assembly. Of particular interest are colloidal crystals, whose optical properties can generate iridescent colours, and provide a means by which photonic crystals may be produced^(author?)¹, while further applications range from lasers ^(author?)² to display devices ^(author?)³, with recent advances demonstrating tunable colours through control of lattice spacing with an external field ^(author?)⁴. Further to the practical importance of colloidal crystals, their well-defined thermodynamic temperature allows colloidal dispersions to be viewed as mesoscopic ‘model atoms’ ^(author?)⁵.

Recently, the ability to tune the colloid-colloid interactions has led to the observation of a wide variety of structures^{6,7,8,9,10,11}. Of particular interest here, to first order AC electric fields can induce dipolar interactions between the colloidal particles, leading to anisotropic interparticle potentials and exotic crystal structures, some of which are not observed in atomic and molecular systems ^(author?)⁷, while external control of the colloid-colloid interactions allows direct observation of phase transitions¹². Furthermore, direct microscopic observation at the single-particle level allows an unprecedented level of detail to be accessed¹³, opening the possibility of tackling long-standing problems in condensed matter, such as freezing¹⁴.

The introduction of a rotating AC field opens up even more possibilities. In this case, the dipolar interactions lead to an attraction in the plane of rotation and to repulsions above and below. Studies with a rotating magnetic field on granular matter indeed produced disc like patterns consistent with expectations^{15,16}. Unlike granular matter, since colloidal dispersions exhibit Brownian motion, thermodynamic equilibrium structures (ie crystals), may be obtained ^(author?)^{11,17}. In previous work Snoswell *et.al.* ^(author?)¹¹ showed that lattice spacing within quasi-2D colloidal crystals could be controlled *in-situ*, by means of coplanar rotating electric field. The interparticle dipolar interactions in the plane of the electric field may be treated to first order as a circularly symmetric attraction, due to the time averaging effect of a rapidly rotating field (1000Hz) on relatively large particles on the micron lengthscale, where the diffusive timescale is of the order of seconds ^(author?)¹⁸.

In considering the interactions between the particles, the asymmetry between the colloids (10nm-1 μ m) and smaller molecular and ionic species must be addressed. A number

of coarse-graining schemes have been developed where the smaller components are formally integrated out (**author?**)¹⁹. This generates a one-component picture, where only the effective colloid-colloid interactions are considered, and the complexity of the description is vastly reduced. The equilibrium behaviour of the colloids in the original multi-component system may then be faithfully reproduced by appeal to liquid state theory (**author?**)²⁰ and computer simulation (**author?**)²¹. Central to the success of this one-component approach is the use of a suitable effective colloid-colloid interaction $u(r)$.

In this study, we use a simple numerical treatment in which we can predict the lattice spacing in the quasi 2D crystal from the electric field strength. We consider a model system of charged colloids, in a rotating electric field (**author?**)¹¹. By exploiting the knowledge both of the electrostatic repulsions and dipolar attractions, we present a direct, quantitative comparison of a tunable interaction and a material property of the crystalline ‘rafts’ formed. We combine experimental measurements of the crystal lattice constant d as a function of field strength E with Monte-Carlo simulations according to a screened Coulomb repulsion plus dipolar attraction where the only fitting parameter is the Debye screening length.

In the simulations, we use pairwise interactions, in other words we assume that at the higher densities at which the crystalline rafts are formed, the system is still accurately described by interactions calculated for two particles in isolation. We note that deviations from this assumption of pairwise additivity have been measured both in the case of strongly charged colloids (**author?**)²² and in the case of *repulsive* dipolar interactions²³. We further compare simulation results with the minimum of the effective potential, which we take as a measure of the lattice constant of the crystalline rafts, which we also determine from experimental data.

This paper is organised into six sections. In section II we present expressions for the effective interactions between the colloids, summing the attractions and repulsions to provide an effective one-component description of the system. Section III describes our experimental methodology. Section IV outlines the Monte-Carlo simulation technique employed. The comparison of simulation and experimental results is presented in section V and in section VI we extrapolate our findings to maximise the tunability of the crystal lattice constant, which may be useful for applications. We conclude our findings in section VII.

II. THEORY AND MODEL

In the following we will consider a system consisting of two particles in a surrounding medium. We shall assume that these particles are charged, leading to a repulsive interaction, and that the rotating AC electric field induces a dipole moment in the two particles and thus induces an attractive interaction. To describe this system, we start from the Derjaguin, Landau, Verwey and Overbeek (DLVO) approach²⁴, which consists of attractive van der Waals interactions at short range, and long-ranged repulsive electrostatic interactions. The van der Waals interactions are very short-ranged, and are neglected, as electrostatic repulsions inhibit the close approach at which van der Waals interactions become important. We shall therefore assume that the only relevant attractions result from the long-ranged dipolar interactions induced by the rotating electric field.

In the linear Poisson-Boltzmann regime, the electrostatic repulsions may be expressed as a hard core Yukawa, or screened Coulomb interaction²⁴,

$$\beta u_{yuk}(r) = \begin{cases} \infty & \text{for } r < \sigma \\ \beta \epsilon_{yuk} \frac{\exp(-\kappa(r-\sigma))}{r/\sigma} & \text{for } r \geq \sigma \end{cases} \quad (1)$$

where $\beta = 1/k_B T$ where k_B is Boltzmann's constant, T is temperature and σ is the colloid diameter. The potential at contact, $\beta \epsilon_{yuk}$ is given by

$$\beta \epsilon_{yuk} = \frac{Z^2}{(1 + \kappa\sigma/2)^2} \frac{l_B}{\sigma} \quad (2)$$

where Z is the colloid charge, l_B is the Bjerrum length and $\kappa = \sqrt{4\pi l_B \rho_i}$ is the inverse Debye screening length where ρ_i is the total number density of monovalent ions.

Now the regime of linear Poisson-Boltzmann theory in which equation (1) holds corresponds to relatively weak charging. Although this is not the case here, a potential of the Yukawa form is recovered at larger separations, if a smaller, renormalized charge is considered (**author?**)²⁵. We tabulate measurements of the ζ -potential of dilute suspensions in table I. These values suggest that we expect a renormalised charge, in the conditions under which the colloids form the crystalline rafts, rather high colloid concentration, hence high counter ion concentration^{18,25}. Therefore, noting that the Debye length is much smaller than the colloid radius, we follow Bocquet *et. al.*²⁶ and take the following expression for the renormalised charge Z_{eff} :

$$Z_{eff} = \frac{4\sigma (1 + \kappa\sigma/2)^2}{l_B (1 + \kappa\sigma)} \quad (3)$$

which we substitute for Z in equation (2). This expression gives good agreement with measurements of the effective colloid charge for particles with a comparable ζ -potential²⁷. We recall that many-body effects can lead to a density-dependence in the effective colloid-colloid interactions (**author?**)^{22, 23}. However, we shall neglect these effects in the present work.

The attractive potential between the colloids resulting from the rotating AC electric field is treated to first order as a dipolar interaction:

$$u_{dip}(r) = \frac{(p \times p)}{2\pi\epsilon\epsilon_0 r^3} \quad (4)$$

where p is the induced dipole moment of each particle, ϵ is the dielectric constant and ϵ_0 is the permittivity of free space. The dipole moment may be calculated from the strength of the electric field

$$p = \frac{1}{2}\pi\epsilon\epsilon_0\sigma^3 K \underline{E} \quad (5)$$

where K is the Clausius-Mosotti factor and takes values between 1 and -1/2 depending upon the origin of the dipole moment. We note that in this case of an alternating field, the root-mean-square of the time dependent field is taken. Substituting $r = \sigma$ leads us to a potential at contact

$$\epsilon_{dip}(\sigma) = \frac{(p \times p)}{2\pi\epsilon\epsilon_0\sigma^3} \quad (6)$$

which has a cubic dependence on the colloid diameter, in the case of all other contributions being unchanged.

In considering the value of the Clausius-Mosotti factor, two regimes are relevant, corresponding to applied electric fields of high and low frequency, in which the dipolar interactions result from dielectric permittivity differences between the particles and the solvent and differences in conductivity respectively⁶. The crossover frequency ω^* between these regimes is given by

$$\omega^* = \frac{1}{2\pi\epsilon_0} \sqrt{\frac{s_p^2 - 2s_p s_m + 2s_m^2}{\epsilon_p^2 - \epsilon_p \epsilon_m + 2\epsilon_m^2}} \quad (7)$$

where s are conductivities and the indices p and m refer to the colloidal particles and the medium respectively. Following **(author?)**²⁸ the conductivity of the particles s_p is taken to be the sum of the bulk conductivity $s_b \approx 0$ and the conductivity on the surface s_s .

$$s_p = s_b + s_s \sigma \quad (8)$$

In principle equation (8) holds for particles larger than $1 \mu\text{m}$. In the case of much smaller particles, one should take into account that the contribution of the diffuse layer to the conductivity of the particles. Noting that the smallest particles used in the experiments are 757 nm in diameter and that the conductivity of the de-ionised water is relatively low, neglect the double layer contribution and thus use equation (8). Since the largest particles studied are 2070 nm in diameter and the frequency is 1 kHz and the bulk ionic strength is $0.01 - 0.1 \text{ mMol}$ as determined from conductivity measurements, we work in the low frequency regime where the contributions from the conductivities dominate **(author?)**²⁸. The Clausius-Mosotti factor therefore takes the following form:

$$K_s = \frac{s_p - s_m}{s_p + 2s_m} \quad (9)$$

Due to the surface conductivity, s_p is much larger than the conductivity of the medium s_b . The value of K_s is therefore close to one. We now combine the contributions from the electrostatic repulsions and the dipolar attractions, yielding the expression.

$$u_{tot}(r) = u_{yuk}(r) + u_{dip}(r) \quad (10)$$

u_{tot} has the form indicated in Fig. 1. We see a minimum in the potential, which one might expect to provide a first approximation to the lattice constant in the 2D colloidal crystal. In sections V and VI we shall compare this minimum to our simulation results.

III. EXPERIMENTAL

Colloidal crystals underwent self-assembly as a result of an applied electric field. We used anionic, sulphate stabilised polystyrene latex particles, either synthesised using a standard technique, surfactant free emulsion polymerisation **(author?)**²⁹ in the case of $\sigma = 757$ and

945 nm, or particles produced by the same method but purchased from Microparticles GmbH for $\sigma = 1390$ and 2070 nm.

Particle electrophoretic mobility was measured using a Brookhaven Zetaplus light scattering instrument. Particle sizes were determined by scanning electron microscopy, either in-house using a Jeol JSM-6330F, in the case of $\sigma = 757$ and 945 nm or by Microparticles GmbH for $\sigma = 1390$ and 2070 nm are listed in table I. Experiments were performed with dilute aqueous suspensions (0.5-1.5 wt%). Schematics of the experimental set up are shown in Fig. 2 All glass surfaces were chemically washed with 0.1M KOH and washed with copious quantities of MilliQ water. Particles were deionised by direct contact with ion exchange beads before being made up to the desired electrolyte concentration with KCl. Very low salt conditions are required as even moderate (mMol) salt concentrations lead to electrohydrodynamic pattern formation due to ion flow^{30,31}. For further details of the experimental set up and procedure the reader is referred to Snoswell *et. al.*¹¹.

We consider our experiment as a 2D system. However, occasionally we noticed some overlap of the crystalline rafts. We do not include these results in our analysis. In order to treat the system in 2D, one might expect the gravitational length $l_g = k_B T / mg$, where m is the bouyant mass of the particle and g is the acceleration due to gravity, to be much less than some characteristic length such as the particle diameter. Due to the fairly small density mismatch between polystyrene and water, in fact even for the largest particles $\sigma = 2070$ nm, $l_g \approx 0.87\sigma$. However, the dipolar interactions between the particles are attractive in-plane, but strongly repulsive in the vertical direction. This promotes the formation of ‘rafts’ and ‘sheets’, and these large assemblies of many particles have very small gravitational lengths. Thus we argue that the system behaves in a quasi 2D manner. The lattice parameter d was taken as the average of typically ten crystalline ‘rafts’, measured across the ‘raft’, of around ten lattice spacings. The response to changing the electric field strength was determined to be less than 100 ms, we waited 5s after changing the field strength before acquiring data.

IV. MONTE-CARLO SIMULATION

We use standard Monte-Carlo (MC) simulations in the NVT ensemble²¹. The particles interact via equation (10) in two dimensions. To mimic the experiments, we initialise the system in a random configuration at a relatively low concentration, corresponding to an area

fraction $\phi = 0.05 - 0.3$. We confirmed that different area fractions gave indistinguishable results, however smaller area fractions often led to longer equilibration times. The attractive interactions cause the particles to approach one another, and form crystallites which then coalesce to form a crystalline ‘rafts’ which contain of order 100 particles, in a qualitatively similar way to the experimental system. Each simulation was equilibrated for typically 30000 MC moves per particle, followed by 3000 production moves per particle. We recall that a potential of the form $1/r^3$ converges in 2D. The lattice constant for this 2D hexagonal crystal was taken as

$$d = \frac{\int_0^b r g(r) dr}{\int_0^b g(r) dr} \quad (11)$$

where $g(r)$ is the pair correlation function, and b the minimum between the first and second peaks of $g(r)$.

We found that when we used $N < 200$, that typically one crystalline domain was formed, around the centre of the simulation box. We therefore do not use periodic boundary conditions, and consider the lattice spacing of the single crystal formed in the simulation. One parameter is the number of particles typically present in each crystalline domain. This is estimated to be around $N = 100 \pm 25$ from experimental data (see Fig. 3). This value is governed by the overall concentration of the colloidal suspension. We have considered the effects of varying N as shown in Fig. 4. The results of a considerable range of N resulted in a variation of d around one percent in d for the $\sigma = 945$ nm system for a field $E = 20$ kVm^{-1} . Each simulation was repeated four times except $N = 576$. We found a slight trend to tighter binding for larger N , however, as shown in Fig. 4, this effect is rather small. We henceforth use one simulation per state point unless otherwise stated. The slight scatter in the simulation data is perhaps indicative the existence of different ‘magic numbers’ for these crystalline rafts³². These may be thought of as 2D hexagonal clusters, whose ‘magic numbers’, ie low energy states, are expected to include 7, 19, 37... Close to a ‘magic number’ the binding may be expected to be relatively tighter. A more detailed exploration of this phenomenon lies beyond the scope of this work. Overall, the variation in d as a function of N is smaller than the experimental scatter, nonetheless we take both $N = 72$ and $N = 144$ values for d when comparing with experimental data. The slightly larger value for $N = 32$ in Fig. 4 is attributed to the small size of the crystalline ‘raft’, such that the surface particles

which are more widely spaced make a greater contribution. The domain size is of order 100 particles, thus, for larger N , defects and grain boundaries may lead to a smaller contribution to the measurement of d . This also applies to experimental data.

For fitting, all parameters are known, except the Debye length κ^{-1} which we take as a free parameter for each particle size and salt concentration, although we note that the effective colloid charge is itself a function of the Debye length, equation (3). It has previously been shown that comparison of simulation and experimental data can yield a reasonable *local* measure of the Debye length³³. Furthermore, in the region of the sample in which the electric field is applied, the colloid volume fraction is much higher, and due to the colloidal counter-ions the ionic strength may increase, leading to a reduction in the Debye length with respect to the bulk. However, it is the Debye length in this region which is relevant for the effective colloid-colloid interactions. The bulk Debye length that may be determined, for example from conductivity measurements, may therefore be taken only as an upper bound. System parameters for different particle sizes are tabulated in table I, and the Debye length is plotted in Fig. 5(a) and the contact potential of the Yukawa interaction [equation (2)] in Fig. 5(b) are plotted as a function of particle diameter.

Clearly, our MC simulations may be expected to provide a reasonable treatment of the crystalline rafts in (quasi) equilibrium, rather than to describe the formation process. We therefore restrict our analysis to a simple characterisation of the crystal rafts, and primarily consider the lattice spacing. We furthermore note both here and in previous work¹¹ that considerable variation in shapes of crystalline rafts was observed, but that this had little impact upon the measurement of the lattice spacing d . Likewise, at the level of this work, we neglect possible local variations in d due to the proximity of an interface. In any case we note that for display applications, all lattice spacings contribute to the diffraction. A few words on equilibration are in order. This applies both to the experimental system, and to the simulations. Neither system is strictly in equilibrium, in that case we might expect a rather regularly-shaped raft such as a hexagon. However, the insensitivity of the lattice parameter either as a function of N (Fig. 4), and the very close agreement between statistically independent simulation runs lead us to conclude that our approach is sufficient to compare lattice parameters between experiment and simulation.

V. RESULTS

The effect of changing the electric field strength is readily demonstrated in Fig. 3, which shows optical microscope images of the region of the sample in which the field is applied. Two field strengths are shown, 29 kVm^{-1} (a) and 80 kVm^{-1} (b) for $\sigma = 945 \text{ nm}$ and we see a correspondingly tighter lattice in the case of the higher field strength. Similar behaviour was observed in¹¹. Figure 3(c) illustrates simulated coordinates for $\varepsilon_{yuk} = 5.78 \times 10^3 k_B T$, $\kappa\sigma = 28.4$, $\varepsilon_{dip} = 50.1 k_B T$, which corresponds to $E = 29.0 \text{ Vm}^{-1}$ for the $\sigma = 945 \text{ nm}$ system (see table I).

A more quantitative comparison between experiment and simulation is shown in Fig. 6, which plots the radial distribution function $g(r)$. We see that the structure appears to be crystalline, with reasonably long-ranged correlations, although, as is clear from Fig. 3, the system is too small to test for truly long-ranged order. We thus note that it is difficult to distinguish the true crystal from a hexatic phase in this system. However, our motivation is to model the experimental system, with $N = 100 \pm 25$ and thus we argue that identification of the hexatic phase lies beyond the scope of this work.

Having illustrated the general behaviour of the system, we now turn our attention to the fitting of the experimental data, with the model described in section II. The experimental data was fitted to the theory by taking the Debye-length as the fitting parameter.

The main results are shown in Figs. 7 and 8 for $\sigma = 757$ and 945 nm , and $\sigma = 1390$ and 2070 nm systems respectively. These concern the lattice parameter d as a function of applied field strength E . In general, the simulation is able to capture the behaviour of the system in a reasonably quantitative manner. Furthermore, simply plotting the minimum in the potential u_{min} given by equation (10) provides a first approximation to the lattice constant d . Figure 7(a) shows the results for $\sigma = 757 \text{ nm}$ particles. Due to the small particle size, and the inverse cubic dependence of the strength of the dipolar attractions on the particle diameter, as characterised by ε_{dip} [equation (6)] the attraction for a given field strength is comparatively small, so we find relatively larger lattice parameters for this system. At low field strengths ($E < 20 \text{ kVm}^{-1}$) we see an increase of the lattice constant for both the experimental data and the simulation, compared to the minimum in the potential. Apparently, as the crystal approaches melting, fluctuations become more pronounced, leading to an increase in d , which is not captured in equation (10), or perhaps a molten surface layer increases the apparent

value of d . We leave this intriguing question for further investigations. Meanwhile, at high field strengths, we find some deviation between simulation, experiment and equation (10). Apparently, due to the long ranged nature of the interaction, second nearest neighbours experience an attraction of sufficient strength that the crystal is compressed by its own cohesion, leading to a smaller lattice constant.

In the case of the $\sigma = 757$ nm particles, we find that for small field strengths, ($E = 10$ kVm^{-1}), the system does not form crystallites, rather it remains as a colloidal liquid. We determined this both by experimental observation and with simulations. In the latter case, we identified crystallisation with a splitting in the second peak of the pair correlation function $g(r)$. The kink around $E \sim 20$ kVm^{-1} in Fig. 7 is likely related an artifact of measuring multiple rafts, so defects and grain boundaries contribute to the value of d . At weak field strengths the rafts tend to be smaller, thus increasing this effect.

At larger particle sizes, (Fig. 8), we again see reasonable agreement between experiment and simulation, albeit with some deviation between simulation and equation (10) at higher field strengths, as the simulation predicts a smaller lattice constant than that observed in the experiments. However, for the $\sigma = 1390$ nm system in particular, in fact equation (10) provides a more accurate description of the experimental data. Apparently some of our assumptions in the simulations, perhaps that of pairwise additivity, begin to break down at high field strengths. According to equation (10), the potential at the minimum of the attractive well is some $250 k_B T$ for an applied field of 50 kVm^{-1} for $\sigma = 1390$ nm. Thus we conclude that for moderate interaction strengths, equation (10) provides a reasonable description of the system.

We now consider the dependence of the system upon the colloid diameter σ . Firstly, we see from Fig. 5(a) that the absolute value of the (fitted) Debye length κ^{-1} does not change significantly for all the four particle sizes studied. Thus, the reduced inverse Debye length $\kappa\sigma$ is linear in σ . The contact potential $\beta\epsilon_{yuk}$ has an approximately inverse cubic dependence on σ for $\kappa\sigma \gg 1$, equation (2), but also depends upon the (effective) charge Z_{eff} . Plotting $\beta\epsilon_{yuk}$ as a function of σ in Fig. 5(b) we find an approximate power law dependence with an exponent of $b = 0.91 \pm 0.01$.

As noted above, the prefactor of the dipolar attraction, ϵ_{dip} [equation (6)], has a σ^{-3} dependence. Although the electrostatic interactions are non-negligible, we nonetheless expect from equation (6) that upon decreasing σ we find a relatively larger lattice constant

for a given field strength, and that larger field strengths are required to provide sufficient interactions that the crystalline rafts form. This we indeed find, as shown in Figs. 7 and 8, and also in the next section.

VI. OPTIMISING THE TUNABILITY

Now we have noted that this system has optical display applications, due to the possibility of externally tuning the lattice parameter d . These applications may be most usefully realised when the possibility to tune the system is maximised, ie when the range of d is maximised. We are therefore motivated to consider a range of particle sizes, and calculate the range of tunability of d . Now σ sets a lower bound to d while the upper bound is set by the melting transition which can be determined by Monte-Carlo simulation.

Hitherto, we have used the Debye length κ^{-1} as a fitting parameter. However, as Fig. 5(a) shows, there is relatively little change in the absolute value of the Debye length for the range of colloid diameters investigated. We therefore fix $\kappa^{-1} = 40$ nm and vary the colloid size, and apply the same methodology as that outlined in sections II and IV, in calculating the response for $\sigma = 400 - 2000$ nm colloids to an external electric field. While an accurate determination of the melting transition is complicated by the small system size, melting is approximately determined by the splitting of the second peak in the radial distribution function $g(r)$ ³⁴. We decrease the electric field to identify the weakest field at which the second peak in $g(r)$ exhibits clear splitting [Fig. 9(a), inset], thus yielding $d(E_{min})$, the lattice spacing just prior to melting. The melting value of the lattice parameter d_m is taken as

$$d_m = d(E_{min}) + \frac{d(E_{min} + \delta E)}{2} \quad (12)$$

where δE is the amount by which the field strength is varied between simulations, typically $0.5 - 1.0$ kVm⁻¹. The error in d_m is then taken as $d_m - d(E_{min})$.

In terms of the particle diameter, d_m grows considerably at small sizes, as the relatively larger Debye length leads to a minimum in the effective potential at relatively larger distances. However, we recall that our analysis suggests a roughly σ^3 dependence of ϵ_{dip} the strength of the dipolar attraction. This suggests that we might expect a stronger electric field to be required for relatively small colloids, and indeed we find that a higher field is

required to provide sufficient cohesive energy to hold the colloids together in the crystal-like ‘rafts’, so at 100 kVm^{-1} , a value we take as a reasonably accessible maximum field strength, the lattice spacing is still around $d_{100} \approx 1.6\sigma$ for $\sigma = 400 \text{ nm}$, where d_{100} is the lattice spacing corresponding to a field strength of 100 kVm^{-1} . Conversely, at larger particle sizes, the Debye length is relatively small, so we find, even at melting, that the lattice constant only approaches around 1.2σ . We note that, at high field strengths, the assumptions of Section II will ultimately break down. The results presented in Figs. 7 and 8 show that $E < 100 \text{ kVm}^{-1}$ is reasonable, at least for $\sigma > 757 \text{ nm}$, supporting our conclusion of a maximum in tuneability around 1.2σ . We show the values of the well depth of equation (10) at melting for the different experimental system in table I, which indicates a trend towards deeper wells for larger particles, i.e. shorter ranges of the repulsive interaction relative to the particle size.

Larger field strengths may be expected to yield greater tunability for the small particle sizes. Since the overall minimum lattice spacing is $d = \sigma$, in principle smaller particles have greater tunability, however experimental observations reveal intense fluid turbulence disrupts crystal formation at higher field strengths. This is caused by large field gradients at the electrode edges that induce strong dielectrophoretic forces. In addition, higher field strengths can cause bubble formation by electrolysis and electrochemical degradation of the electrodes.

The result is thus that intermediate particle sizes have the highest degree of tuneability, for a given maximum field strength. Here we have considered 100 kVm^{-1} , which leads to a maximum tuneability of d_m/d_{100} in the range $1000 \text{ nm} < \sigma < 1500 \text{ nm}$.

VII. CONCLUSIONS

2D Colloidal crystalline ‘rafts’ with externally controllable properties have been modeled with Monte-Carlo simulations, and the resulting lattice constant, both experimental and simulated, has been compared to the minimum in the effective interaction potential. In treating the effective colloidal interactions, we find that a straightforward, pairwise approach provides a reasonable description in describing the lattice parameter. The minimum in the effective interaction formed from combining the electrostatic repulsions and dipolar attractions is a useful means to approximate the lattice parameter, although close to melting fluctuations

lead to a larger value in the lattice parameter than this minimum. Conversely, at high field strengths, our treatment appears to be less accurate. Apparently, higher order terms which we have not accounted for may become important, such as non-linear Poisson-Boltzmann contributions to the electrostatic interactions, leading to a deviations from the Yukawa form [equation (1)]²² or limitations in our pairwise treatment of the dipolar attractions²³. Other possibilities include inaccuracies in our assumptions for the effective colloid charge [equation (3)], limitations of the 2D behaviour of the experimental system. Perhaps due to a cancellation of errors, at high field strengths, the minimum in the effective interaction can sometimes provide a more accurate value of the lattice parameter than the simulations.

Another important assumption lies in our derivation on the electrostatic interactions. While their Yukawa-like form is well-accepted²⁵, the values the effective colloid charge comes from equation (3). We note that the Debye length we determine seems rather constant across the four particle sizes considered, [Fig.5 (a)], which suggests that our approach is at least consistent. However challenging it may be, a more quantitative measurement of the local ion concentration in the vicinity of the crystalline rafts is desirable and will be considered in the future. Furthermore, there may be some variation in the value of Z_{eff} . In fact this should affect all state points in a similar manner (for each particle size), and therefore we anticipate a similar outcome, but that a different value might be arrived at in the fitting of the Debye length, however, owing to the relatively short-ranged nature of the interaction, the effect of a different value for the effective charge is unlikely to impinge significantly the Debye length and should have a negligible effect on our main results.

We have also assumed that a given system is described by *one single* Debye length. In fact, in the counterion-dominated regime, the Debye length is in fact a function of colloid concentration³⁵, an effect we have neglected. This might lead to a tightening at higher colloid concentration (i.e. high field strength), which may be expected to lead to an increase in deviation with the experimental results (Figs. 7 and 8). Nevertheless, varying the Debye length as a function of local colloid concentration would be worth considering in the future.

We have extended our approach a range of colloid size, to optimise the lattice tuneability for display applications. Tunable 2D crystal rafts can behave as tunable diffraction gratings capable of filtering white light into visible colours(**author?**)¹¹. Similar tunable diffraction has been proposed for display devices³⁶. The range of colours obtainable for a given geometry is governed by the lattice tunability. Fig 9b demonstrates that lattice tunability in our sys-

tem is maximised for particles of approximately 1 to 1.5 microns. Only higher field strengths applied to smaller particles can increase the lattice tunability. As already indicated, higher field strengths are not practical in the current experimental system, however in future experiments metal coated colloids would exhibit much stronger dipolar interactions, enabling a reduction in field strength for a given attraction. Regardless, our methodology illustrates using the well-developed machinery of effective colloidal interactions, as a means to model potentially complex interactions, useful for engineering purposes.

-
- * Electronic address: paddy.royall@bristol.ac.uk
- † VDL, Fuchstan str. 61, Frankfurt am Main, 60489, Germany.
- ¹ Joannopoulos, J., Villeneuve, P. & Fan, S. Photonic crystals: putting a new twist on light. *Nature* **386**, 143–149 (1997).
- ² Colombelli, R. *et al.* Quantum cascade surface-emitting photonic crystal laser. *Science* **302**, 1374–1377 (2003).
- ³ Arsenault, A. C., Miguez, H., Kitaev, V., Ozin, G. A. & Manners, I. A polychromic, fast response metallopolymer gel photonic crystal with solvent and redox tunability: A step towards photonic ink (p-ink). *Advanced Materials* **15**, 503–507 (2003).
- ⁴ Arsenault, A. C., Puzzo, D. P., Manners, I. & Ozin, G. A. Photonic-crystal full-colour displays. *Nature Photonics* **1**, 468–472 (2001).
- ⁵ Pusey, P. N. *in Liquids, Freezing and the Glass Transition*, eds Hansen, J. P., Levesque, D. and Zinn-Justin, J. (North-Holland, Amsterdam, 1991).
- ⁶ Jones, T. B. *Electrohydrodynamics of Particles* (Cambridge University Press, 1995).
- ⁷ Yethiraj, A. & van Blaaderen, A. A colloidal model system with an interaction tunable from hard sphere to soft and dipolar. *Nature* **421**, 513–517 (2003).
- ⁸ Manoharan, V. N., Elessor, M. T. & Pine, D. J. Dense packing and symmetry in small clusters of microspheres. *Science* **301**, 483–487 (2003).
- ⁹ Martin, S., Bryant, G. & van Megen, W. Observation of a smecticlike crystalline structure in polydisperse colloids. *Phys. Rev. Lett.* **90**, 255702 (2003).
- ¹⁰ Leunissen, M. E. *et al.* Ionic colloidal crystals of oppositely charged particles. *Nature* **437**, 235 (2005).
- ¹¹ Snoswell, D. R. *et al.* Dynamic control of lattice spacing within colloidal crystals. *New Journal of Physics* **8**, 267 (2006).
- ¹² Yethiraj, A., Wouterse, A., Groh, B. & van Blaaderen, A. Nature of an electric-field-induced colloidal martensitic transition. *Phys. Rev. Lett.* **92**, 058301 (2004).
- ¹³ van Blaaderen, A. & Wilzius, P. Real-space structure of colloidal hard-sphere glasses. *Science* **270**, 1177 (1995).
- ¹⁴ Gasser, U., Weeks, E. R., Schofield, A., Pusey, P. N. & Weitz, D. A. Real-space imaging of

- nucleation and growth in colloidal crystallization. *Science* **292**, 258 (2001).
- ¹⁵ Halsey, T. C., Anderson, R. A. & Martin, J. E. The rotary electrorheological effect. In Bulough, W. (ed.) *Proceedings of the Fifth International Conference on Electrorheological Fluids, Magneto-Rheological Suspensions and Related Technology*, 192–200 (World Scientific, Singapore, 1995).
- ¹⁶ Martin, J. E., Anderson, R. A. & Tigges, C. P. Thermal coarsening of uniaxial and biaxial field-structured composites. *J. Chem. Phys.* **110**, 4854–4866 (1999).
- ¹⁷ Lumsdon, S. O., Kaler, E. W., P., W. J. & Velev, O. D. Dielectrophoretic assembly of oriented and switchable two-dimensional photonic crystals. *Applied Physics Letters* **82**, 949–951 (2003).
- ¹⁸ Russell, W., Saville, D. & W.R., S. *Colloidal Dispersions* (Cambridge Univ. Press, Cambridge, 1989).
- ¹⁹ Likos, C. Effective interactions in soft condensed matter physics. *Physics Reports* **348**, 267–439 (2001).
- ²⁰ Hansen, J.-P. & Macdonald, I. *Theory of Simple Liquids* (London: Academic press, 1976).
- ²¹ Frenkel, D. & Smit, B. *Understanding Molecular Simulation: from Algorithms to Applications* (New York: Academic, 2001).
- ²² Brunner, M., Bechinger, C., Strepp, W., Lobaskin, V. & von Gruenberg, H. H. Density-dependent pair interactions in 2d. *Europhys. Lett.* **58**, 926–965 (2002).
- ²³ Zahn, K., Maret, G., Russ, C. & von Gruenberg, H. Three-particle correlations in simple liquids. *Phys. Rev. Lett.* **91**, 115502 (2003).
- ²⁴ Verwey, E. & Overbeek, J. *Theory of the Stability of Lyophobic Colloids* (Elsevier, Amsterdam, 1948).
- ²⁵ Alexander, S. *et al.* Charge renormalisation, osmotic-pressure, and bulk modulus of colloidal crystals - theory. *J. Chem. Phys.* **80**, 5776–5781 (1984).
- ²⁶ Bocquet, L., Trizac, E. & Aubouy, M. Effective charge saturation in colloidal suspensions. *J. Chem. Phys.* **117**, 8138–8152 (2002).
- ²⁷ Yamanaka, J., Matsuoka, H., Kitano, H. & Ise, N. Revisit to the intrinsic viscosity-molecular weight relationship of ionic polymers. *Journal of Colloid and Interface Science* **134**, 92–106 (1990).
- ²⁸ Ermolina, I. & Morgan, H. The electrokinetic properties of latex particles: comparison of electrophoresis and dielectrophoresis. *Journal of Colloid and Interface Science* **285**, 419–428

- (2005).
- ²⁹ Goodwin, J. W., Hearn, J., Ho, C. C. & Ottewill, R. The preparation and characterization of polymer lattices formed in the absence of surface active agent. *British Polym. Journal* **5**, 347–362 (1973).
- ³⁰ Isambert, H., Ajdari, A., Viovy, J.-L. & Prost, J. Electrohydrodynamic patterns in charged colloidal solutions. *Phys. Rev. Lett.* **78**, 971–974 (1997).
- ³¹ Lumsdon, S. O., Kaler, E. W. & Velev, O. D. Two-dimensional crystallization of microspheres by a coplanar ac electric field. *Langmuir* **20**, 2108–2116 (2004).
- ³² Wales, D. J. *Energy Landscapes: Applications to Clusters, Biomolecules and Glasses* (Cambridge University Press, Cambridge, 2004).
- ³³ Royall, C., Leunissen, M., Hynninen, A.-P., Dijkstra, M. & van Blaaderen, A. Re-entrant melting and freezing in a model system of charged colloids. *J. Chem. Phys.* **124**, 244706 (2006).
- ³⁴ Truskett, T. M., Torquato, S., Sastry, S., Debenedetti, P. G. & Stillinger, F. H. Structural precursor to freezing in the hard-disk and hard-sphere systems. *Phys. Rev. E* **58**, 3083–3088 (1998).
- ³⁵ Rojas, L. F., Urban, C., Schurtenberger, P., Gisler, T. & von Gruenberg, H. H. Reappearance of structure in colloidal suspensions. *Europhys. Lett.* **60**, 802–808 (2002).
- ³⁶ Aschwanden, M. & Stemmer, A. Low voltage, highly tunable diffraction grating based on dielectric elastomer actuators. *Proc. SPIE* **6524**, 65241N (2007).

diameter (nm)	Effective Yukawa contact potential $\beta\epsilon$	$\kappa\sigma$	Ionic strength (mMol)	ζ potential (mV)	melting well depth ($k_B T$)
757±86	4.60±0.05×10 ³	19.0±1.0	0.06±0.01	-34.0 ± 1.4	2.7±0.1
965±44	5.78±0.02×10 ³	28.4±2.0	0.08±0.01	-37.1 ± 1.4	2.9±0.1
1390±30	8.27±0.05 × 10 ³	32.3±3.0	0.05±0.005	-39.9 ± 2.0	3.1±0.1
2070±40	1.17±0.01 × 10 ⁴	38.8±3.0	0.04±0.005	-43.6 ± 2.4	3.4±0.1

Table I: Fitted parameters of the Debye screening length used in the MC simulations for systems with different colloid diameters. Errors in the diameter are standard deviations in the data obtained found from electron microscopy measurements, while those in $\beta\epsilon$, $\kappa\sigma$, and the ionic strength are estimated from the fitting of d from MC data. ζ potential measurements were made in a 0.01 mMol KCl solution

Acknowledgments We thank Jeremy Baumberg, Martin Cryan, Daan Frenkel and Junpei Yamanaka for helpful discussions. CPR acknowledges the Royal Society for funding and Hajime Tanaka for kind provision of lab space and computer time. DES thanks Kodak European Research Centre, Cambridge and EPSRC (EP/DO33047/1) for funding.)

Figure 1: The interaction potentials considered in this system. The Yukawa repulsion $u_{yuk}(r)$ models the electrostatic repulsions [dotted line, equation (1)], the dipolar attractions are plotted as $u_{dip}(r)$ dashed line, [equation (4)]. These are combined to yield the total potential $u_{tot}(r)$, solid gray line (equation 10). This figure corresponds to a particle diameter of $\sigma = 757$ nm and a field strength $E = 30$ kVm^{-1}

Figure 2: A schematic of the experimental set-up, side view (a) and plan view (b). The electric field is assumed to be constant across the observation region, as shown in (b). (b) depicts the quadrupolar electrode configuration (a,b),(c,d)

Figure 3: Images of crystal rafts for the $\sigma = 945$ nm system for applied fields of 29.0 and 80.0 kVm^{-1} for **a** and **b** respectively. Scale bars= $10 \mu m$. **c** snapshot from MC simulation for same system for a field of 30.0 kVm^{-1} and $N=144$.

Figure 4: Change in the lattice constant for simulated systems of different sizes. Here $\sigma = 945 \text{ nm}$ and a field strength $E = 20 \text{ kVm}^{-1}$. Each run was repeated four times except $N = 576$. Error bars denote standard deviations over the results from different runs. Dashed line is solely a guide to the eye.

Figure 5: (a) The Debye length κ^{-1} fitted from Monte-Carlo simulation as a function of particle size. Dotted line denotes $\kappa^{-1}=40 \text{ nm}$ taken for the simulations in section VI. Error bars denote the uncertainty in the Debye length resulting from the fitting in Figs. 7 and 8. (b) The contact potential of the Yukawa interaction $\beta\varepsilon_{yuk}$ [equation (2)] as a function of particle size. We include $\sigma = 400 \text{ nm}$ for which we take the Debye length $\kappa^{-1} = 40 \text{ nm}$.

The straight line is fit of the function $\beta\varepsilon_{yuk}(\sigma) = A\sigma^b$ where the fitted parameters are

$$A = 11.1 \pm 1.1 \text{ and } b = 0.91 \pm 0.01.$$

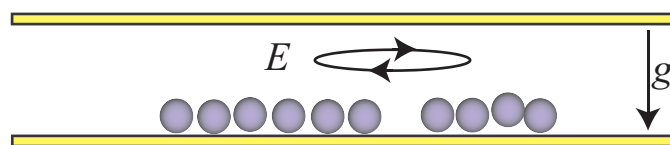
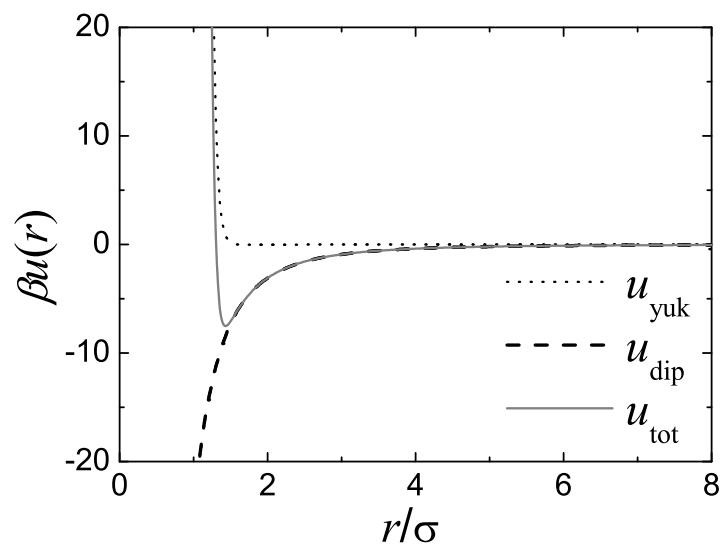
Figure 7: Experimental results compared to MC simulation and the minimum in the effective potential. **a** 757 nm and **b** 945 nm diameter colloids. Filled squares are $N = 72$ while crossed are $N = 144$ from MC simulation. Circles are experimental data. Grey lines are the minimum of equation 10. Error bars in the experimental data are standard deviations.

Figure 8: Experimental results compared to MC simulation and the minimum in the effective potential. **a** 1390 nm and **b** 2070 nm diameter colloids. Filled squares are $N = 72$ while crossed are $N = 144$ from MC simulation. Circles are experimental data. Grey lines are the minimum of equation 10. Error bars in the experimental data are standard deviations.

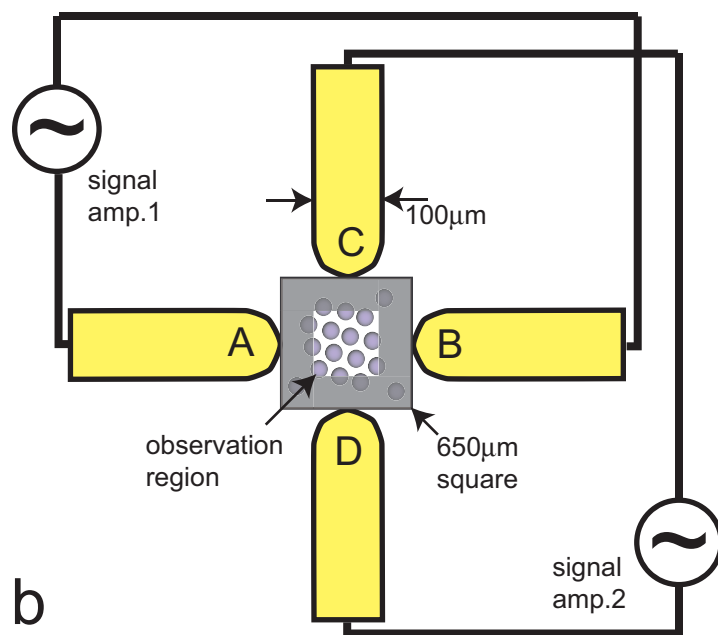
Figure 9: (a) The lattice spacing around melting (dm , filled squares), and at at applied field of 100 kVm^{-1} , as determined from MC simulation (crosses) and from Equation 10, as a function of particle size. Inset shows a radial distribution function close to melting ($\sigma = 1000 \text{ nm}$, $E = 11.0 \text{ kVm}^{-1}$). Arrow indicates split second peak.

(b) the tunability ratio as a function of particle size. Connecting lines are guides to the eye.

Figure 6: Radial distribution functions for an applied field of $E=30.7 \text{ kVm}^{-1}$ for the $\sigma = 2070 \text{ nm}$ system. Circles are experimental data, line is MC simulation for $N=144$. Arrows denote the first few peaks of a hexagonal lattice, $d, \sqrt{3}d, 2d, \sqrt{7}d, 3d\dots$



a



b

